JOURNAL OF APPLIED ELECTROCHEMISTRY 16 (1986) 636–642

Factors affecting the discharge lifetime of lithium–molten nitrate thermal battery cells using soluble cathode materials

G. E. McMANIS, A. N. FLETCHER, M. H. MILES

Energy Chemistry Branch, Chemistry Division, Research Department, Naval Weapons Center, China Lake, California 93555, USA

Received 16 July 1984

The use of soluble cathode materials in molten nitrate electrolyte thermal battery cells presents several problems related to cathode material diffusion into the anolyte. A chemical reduction of the soluble cathode material by molten lithium anodes is observed to degrade cell performance. Factors affecting cell lifetime were found to include discharge rate and temperature, cell thickness, activation into load versus open circuit and the presence or absence of a Cl^- rich separator layer.

1. Introduction

The use of soluble cathode materials in molten nitrate electrolytes presents the twofold advantage of high rates and favourable cathode potentials [1–4]. Attendant with these advantages are the parasitic reactions that may occur at the anode surface if the cathode material is allowed to diffuse into the anolyte. This paper characterizes the effect of cathode active material diffusion into the anolyte and identifies a solution leading toward a practical lithium–molten nitrate–soluble cathode thermal battery.

A series of studies [1–4] have identified $AgNO_3$, $Cd(NO_3)_2$ and $Pb(NO_3)_2$ as likely candidates for soluble cathode materials in high-rate Li–$LiNO_3$-electrolyte thermal battery cells. Of these materials, only $AgNO_3$ is observed to form a metallic deposit during high-rate discharge onto nickel or platinum current collectors. One parasitic reaction that degrades cell lifetime results from Ag^+ diffusion to a lithium anode and the chemical reduction of Ag^+ to form Ag^0 on the anode surface. This parasitic reaction in turn decreases the effective anode area by the blocking action of silver metal and thus increases the effective current density and operating overpotential of the anode, decreasing cell voltage, performance (i versus E) and cell lifetime.

The amount of silver required to form a monolayer coverage of the anode is very small compared to the amount required to sustain a thermal battery cell operating at 500 mA cm^{-2} for, say, 90 s. The catholyte silver ion concentration must be very high while the anolyte silver ion concentration must be kept effectively near zero. Maintaining such a concentration gradient while allowing free Li^+ transport across the cell with a minimal cell internal resistance is not a trivial task.

Since the development of lithium–transition metal composite anode materials, high-rate discharges of conventional LiCl–KCl electrolyte cells using FeS_2 cathodes have been reported [5, 6]. This paper focuses on the use of a lithium–iron composite anode material consisting of a homogeneous suspension of elemental lithium on iron particles [5]. These composite anodes have the distinct advantage of giving easily fabricated, readily reproducible anode surfaces at minimal expense. In addition these anodes provide surfaces of essentially pure elemental lithium. Alternative lithium anodes, i.e. Li(Al), Li(B) or Li(Si), provide lithium in an alloyed form at less than unit activity with a concomitant loss in open circuit anode potential.

0021–891X/86 $03.00 + .12

2. Experimental details

2.1. *Anode composite synthesis*

The lithium–iron composite used in this study was prepared in ingot form in an argon atmosphere glove box with H_2O and O_2 concentrations below 10 p.p.m. No N_2 elimination system was available. Ingot preparation consisted of heating 28.0 g of reduced iron powder (−325 mesh, Alfa, reagent grade) in a nickel crucible to 400° C, then 4.0 g of lithium ribbon (99.9%, ROC/RIC) was added and allowed to melt into the iron powder. Any oxide slag remaining was removed with a stainless steel spatula. The composite material was then sintered at 450–500° C for approximately 30 min. This assured uniform contact between the lithium and the iron particles and allowed for the reduction of any transition metal oxides present on the iron particle surface. The composite material was then removed from the crucible, pressed into a nickel mold and allowed to cool. Analysis of the composite formed as described indicated a material 7.5–9.5 wt % lithium (using conventional gasometric techniques involving reaction of the lithium with water to evolve hydrogen). Generally, composite lithium content was a function of the sintering time and temperature; longer or hotter sinterings gave lower net lithium content due to the low surface tension and high vapour pressure of lithium at 500° C. Galvanostatic discharges of the composite material at low rates showed a single inflection in 1 M $LiClO_4$–propylene carbonate with no evidence for any formation of an intermetallic compound. The composite material prepared as described above was formed into a foil of desired thickness by cold rolling followed by cutting to desired anode diameter. All cells used here were 1.27 cm in diameter and 1–2 mm thick.

2.2. *Cell preparation and testing*

Cells were prepared by cold welding discs, 1.27 cm in diameter, of the Li(Fe) composite anode material to iron backings, 0.074 cm thick and 3.2 cm in diameter. The cold welding procedure was adapted from [7]: iron discs were etched in a 1 : 2 solution of concentrated, reagent grade HNO_3 and reagent grade HCl. The discs were then washed repeatedly in milli-Q water and finally dried *in situ* at room temperature. Composite material discs were scraped with a steel scalpel to expose a fresh lithium surface and pressed onto the etched iron backing. This bond was found to retain physical integrity even when the anode was held inverted at 425° C. The completed backed anodes were then transferred to a deaereated (argon saturated) mixture of cyclohexane and pentane for transport to the cell testing device. The use of argon saturated hydrocarbon solvents allowed overnight storage of anodes exterior to the glove box without evidence of film formation. Anodes formed a loose grey film in hydrocarbon solvents that had not been deaerated.

The Li(Fe) anode, like the Li(B) anode, rapidly forms Li_3N inclusions on exposure to dried air containing only traces of H_2O [8]. Thus, all handling procedures were such that the anodes were exposed to air less than 30 s before use.

The remainder of the cell was assembled by techniques described previously. Electrolyte wafers were prepared by dipping discs of Gelman (type A) glass fibre filters in the molten salt or molten salt eutectics. All salts were reagent grade and with the exception of $AgNO_3$ were dried at 120–130° C *in vacuo* overnight. $LiNO_3$ and LiCl were baked at over 150° C for several days *in vacuo* before use. Reagent grade $AgNO_3$ was ground to a fine powder in an agate mortar and pestle but otherwise used as received. Eutectic mixtures were prefused in Pyrex at 300–400° C, ground, baked *in vacuo* at 120–130° C then fused in platinum before use. The cathode electrode (current collector) was a polished nickel disc (0.025 cm thick, 99.99%, ROC/RIC) 3.2 cm in diameter.

Fig. 1 illustrates the cross-section of a typical cell in the final design. The Li(Fe) anode was pressed into the molten electrolyte wafer and thus sealed from the ambient atmosphere. Cells similar to that shown were about 3.0 mm thick. All discharges reported herein are in $mA\,cm^{-2}$ (based upon anode area). Thermal battery cells constructed as described above were discharged at constant current using a PAR (Model 371) potentiostat/galvanostat in a specially designed, inert atmosphere, large diameter cell testing

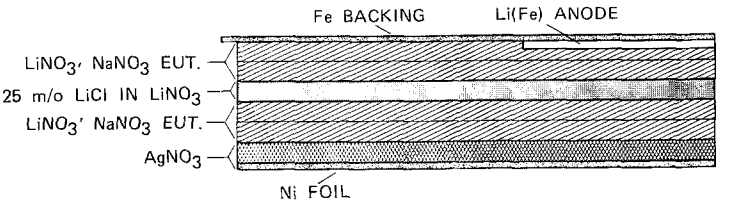

Fig. 1. Cross-sectional view of a typical Li(Fe) thermal battery cell. Nominal thickness is 3 mm; anode area is 1.26 cm^2.

device. This device allowed testing of cells up to 3.2 cm in diameter in an argon atmosphere at temperatures ranging from ambient to 450° C. Fig. 2 shows the device in cross-section.

In a typical operation an anode was placed on the anode heat sink (already at temperature) and lowered to the central region of the furnace with continuous top-down flow of purified argon. Once equilibrated the cathode heat sink was lowered and the layered cell (less the anode) was placed on the cathode heat sink, allowed to equilibrate and raised to the centre of the furnace, so completing the cell.

The thermal history of the cell was monitored using thermocouples in the anode heat sink, on the cathode heat sink or within the cell itself.

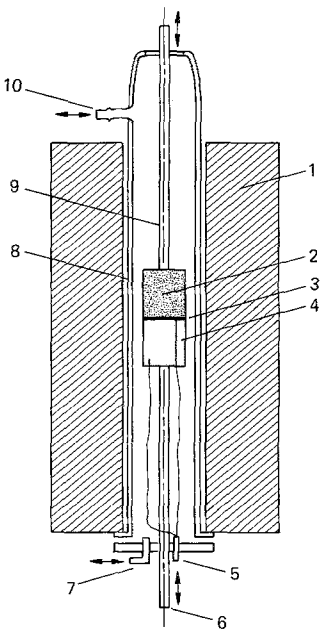

Fig. 2. Inert atmosphere, large diameter cell testing device. 1, Furnace; 2, anode heat sink; 3, thermal battery cell; 4, cathode heat sink; 5, data I/O and thermocouple port; 6, hydraulic ram for cathode heat sink; 7, argon inlet; 8, quartz test chamber liner; 9, anode heat sink ram; 10, top side argon inlet/outlet.

Overall temperature control of ±2° C was achieved through the use of an Omega digital temperature controller in time proportional mode (Model 4001-KC). Thermocouples throughout the tester were monitored using a Fluke (Model 2166A) digital thermometer. Experiment coordination used a Gralab (Model 900) programmable laboratory timer. The data collection system (Hewlett–Packard) has been described previously [9].

3. Results and discussion

Several papers have demonstrated the unusual high rate capability of lithium anodes in molten nitrate electrolytes. Both Li(Fe) and Li(B) anodes show broad flat potentiostatic discharges with a plateau near 1000 mA cm^{-2} for Li(B) at −2.8 V (versus Ag^+/Ag) and a plateau from 2000–3000 mA cm^{-2} for Li(Fe) anodes at the same potential [6].

The rate capability noted in potentiostatic discharges is seldom equalled by larger, less idealized cell designs. Several factors contribute to performance degradation in the scale-up of these cells. One such factor is the increasing importance of the parasitic chemical reduction of the SiO_2 binder. Observed binder degradation becomes severe at higher (over 400° C) temperatures with formation of small nodules of elemental silicon at the periphery of the anode. The reaction for degradation of the binder (Reaction 1) is exothermic with a value of ΔG^0 (300° C) equal to −68.1 kcal mol^{-1}.

$$4Li_{(l)} + SiO_{2(s)} \rightarrow 2Li_2O_{(s)} + Si_{(s)} \quad (1)$$

Another variable that we have found to have an even more profound effect on cell performance and cell lifetime is the migration of the cathode soluble material from the catholyte to the anolyte where reduction by lithium in the anode may take place.

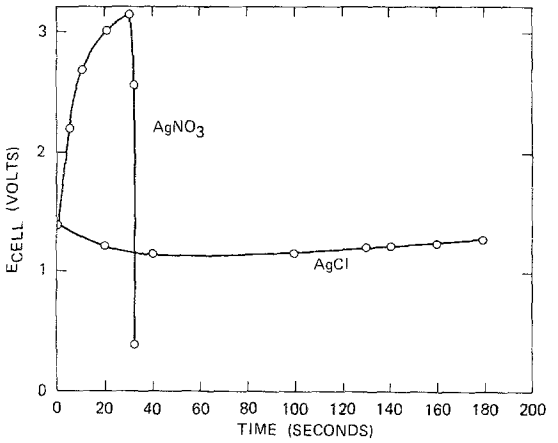

Fig. 3. Li(Fe) thermal battery cells. $LiNO_3$–KNO_3 eutectic electrolyte $AgNO_3$ versus AgCl cathodes. T, 350° C; J, 500 mA cm^{-2}; anode area, 1.26 cm^2.

Although there are solid cathode materials capable of sustaining 500 mA cm^{-2}, there are relatively few that operate with as favourable a potential as that of the Ag^+ cathode. Fig. 3 demonstrates the significant cell voltage penalty incurred on changing from a soluble $AgNO_3$ cathode to a solid (insoluble) AgCl cathode. While the AgCl cell does operate for significantly longer periods, it does so at significantly lower cell potentials. It is apparent that any means of extending the lifetime of the $AgNO_3$ cathode cell would be beneficial to most measures of thermal battery cell performance.

The thermodynamics of the reaction of lithium with Ag^+ are extremely favourable. A graph of anode open circuit voltage (versus Ag^+/Ag reference) in molten $LiNO_3$–KNO_3 as a function of temperature gives a value of ΔG ranging from -74.7 to -79.3 kcal mol^{-1} and a value of ΔS of -11.5 cal mol^{-1} K^{-1}. These values are consistent with the reaction

$$Li_{(l)} + AgNO_{3(l)} \rightarrow LiNO_{3(l)} + Ag^0_{(s)} \quad (2)$$

that yields a value of ΔG^0 of -79.1 kcal mol^{-1} at 350° C and a value of ΔS^0 of -7.8 cal mol^{-1} K^{-1}, where ΔS is the reaction entropy change in the absense of applied current and ΔG^0 is the standard Gibbs free energy change for the reaction.

It is obvious that any Ag^+ ions diffusing into the anolyte would be reduced onto the anode by a displacement reaction with lithium metal. This reduction to Ag^0 on the anode surface lowers the effective anode surface area, thus increasing the effective current density at the anode and raising the overpotential at the anode. In cells where Ag^+ diffusion is present, fine Ag^0 particles have been observed on the anode surface after cell discharge.

A general study of the parameters influencing the diffusion of Ag^+ across the thermal battery cell was undertaken. Fick's law predicts the silver ion flux J_{Ag^+} at some point χ (in the absence of any hydrodynamic mass transport [9]) to be related by

$$J_{Ag^+}(\chi) = -D_{Ag^+} \nabla C_{Ag^+}(\chi) - \frac{F}{RT} D_{Ag^+} C_{Ag^+} \nabla \phi_\chi \quad (3)$$

Assuming a linear electric field gradient (reasonable in the 'bulk' of the cell), Equation 3 may be modified to yield the more tractable equation:

$$J_{Ag^+}(\chi) = -D_{Ag^+} \nabla C_{Ag^+}(\chi) - \frac{F}{RTb} \Delta E D_{Ag^+} C_{Ag^+} \quad (4)$$

where $\Delta E/b$ is the electric field across the cell and b is the cell thickness.

At the cathode one desires the silver reduction reaction concentration overpotential (η_c) to be as close to zero as possible. This concentration overpotential may be expressed by Equation 5 when the cathode reaction is the deposition of an insoluble substance [10].

$$\eta_c = \frac{RT}{nF} \ln \frac{C(\chi = 0)}{C^*} \quad (5)$$

where C^* is the 'bulk' Ag^+ concentration required in the catholyte and n is the number of electrons transferred.

Constant current electrolyses obey the Sand equation as shown in Equation 6, assuming a planar electrode and an unstirred solution [11].

$$C(\chi = 0) = C^* - \frac{2it^{\frac{1}{2}}}{nFAD^{\frac{1}{2}}\pi^{\frac{1}{2}}} \quad (\text{if } t \ll \tau) \quad (6a)$$

$$C(\chi = 0) = 0 \quad (\text{if } t \geqslant \tau) \quad (6b)$$

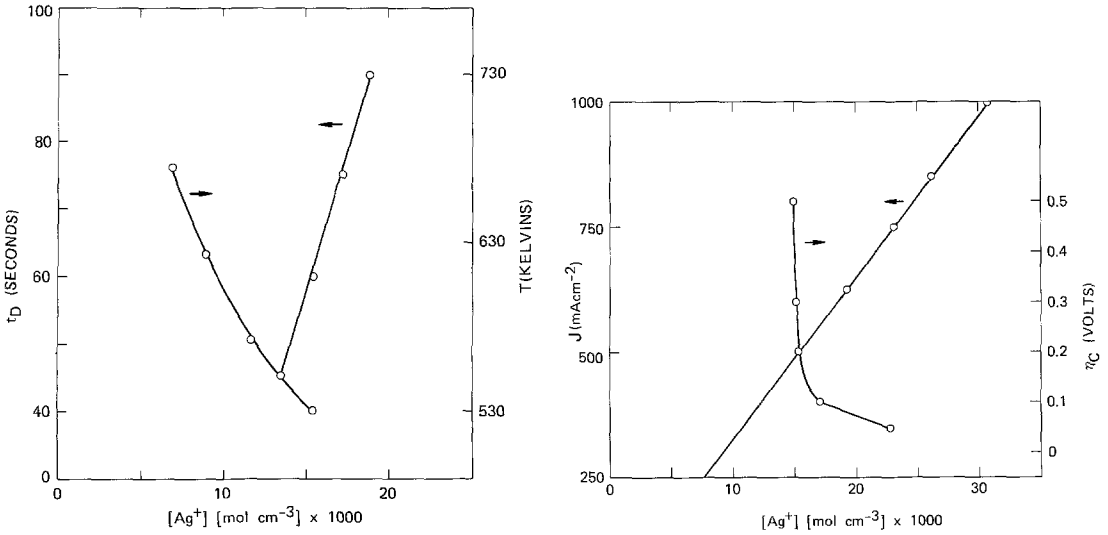

Fig. 4. (a) Effect of discharge time on design concentration of $AgNO_3$ required (T, 257° C; J, 500 mA cm^{-2}; anode area, 1.26 cm^2). Also shown is the effect of temperature on design concentration (t, 60 s; J, 500 mA cm^{-2}; anode area, 1.26 cm^2). Diffusion coefficients are from [12]. (b) Effect of current density and diffusion overpotential on design concentration of $AgNO_3$. Current density study used T, 257° C; t, 60 s; η_c, 0.2 V. The η_c study used T, 257° C; t, 60 s; J, 500 mA cm^{-2}; A, 1.26 cm^2. Diffusion coefficients are from [12].

where τ, the transition time, is when the concentration of the cathode active material (at the electrode surface ($C(\chi = \phi)$) is insufficient to support the current being passed. At that point, the electrode reaction shifts to the next more difficult process [11].

In the design of a thermal battery cell, one would wish to derive a value for C^* as a guideline for the minimum concentration of cathode active material required to meet the discharge criteria of current, maximum cathode overpotential, operating temperature and discharge time. Solving for C^* by substituting Equation 5 into Equation 6a yields Equation 7.

$$C^* \geqslant \frac{2it^{\frac{1}{2}}}{nFAD^{\frac{1}{2}}\pi^{\frac{1}{2}}[1 - \exp(nF\eta_c/RT)]} \qquad (7)$$

It is thus possible to set a value for t equal to the maximum discharge time, and to set a value for T, the diffusion coefficients D, the current density (i/A) and the maximum permissible value of η_c to solve for a C^* that gives a reasonable approximation to the amount of cathode active material necessary to fulfil the design criteria. Data derived from Equation 7 assume a fixed effective electrode surface area over the period of the discharge. This assumption is reasonable in the context of the experiments described here.

In marked contrast to the fine dendritic structures observed in the high-rate deposition of Ag^+ from molten $NaNO_3$–KNO_3 in the absence of binder materials, depositions in actual thermal battery cells (as in Fig. 1) show a much more compact silver mass. In these cells, penetration of the filter paper by the dendrites is not observed. Instead the facial pressure applied to the cell and the physical integrity of the glass fibre filters force dendritic growth to occur in the plane of the cell. Consequently, cathodic silver structures tend to be compact masses of silver as a relatively uniform deposit.

While the uncertainty in the value of A as a function of t prevents quantitative accuracy, physical conditions within the cell allow data gathered from Equation 7 to be considered as a qualitative estimate of C for design purposes. Fig. 4a and b illustrate the relationships among the estimate of C_{Ag+}, a user specified η_c, i, T, t and A. Fig. 4a shows C_{Ag+} as a function of t and T while Fig. 4b shows C_{Ag+} as a function of current density and 'maximum allowable' diffusion overpotential.

Although the data shown in Fig. 4 are valuable in a qualitative sense only, they illustrate

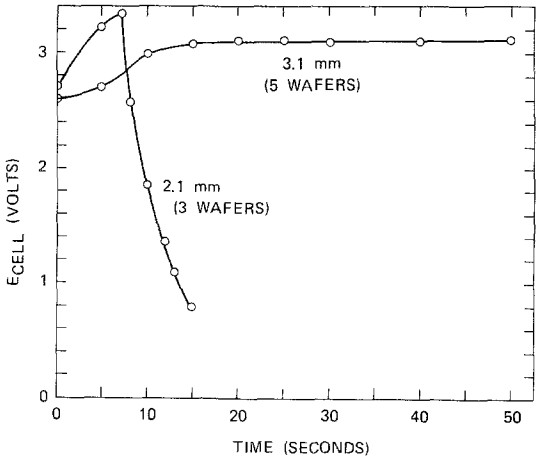

Fig. 5. Effect of increasing cell thickness on cell lifetime 1.26 cm^2, 500 mA cm^{-2}. Cells were Li(Fe)–(Li, Na)NO_3–$AgNO_3$ and used a 25 mol % LiCl in $LiNO_3$ separator wafer.

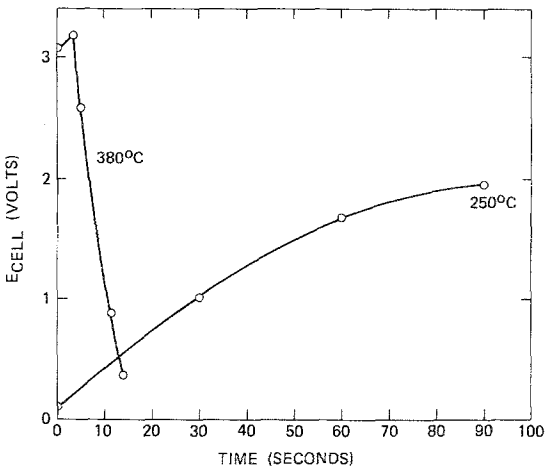

Fig. 6. Effect of temperature on cell lifetime. Identical Li(Fe)–(Li, Na)NO_3–$AgNO_3$ cells. Cells were activated into a 500 mA cm^{-2} load. Cells used a 25 mol % LiCl in $LiNO_3$ separator wafer.

the high concentrations of Ag^+ (or Pb^{2+} or Cd^{2+}) necessary in the catholyte. Those concentrations in turn illustrate the magnitude of the concentration gradient, $\nabla C_{Ag^+}(\chi)$, across a cell less than 3 mm thick. This concentration gradient is of maximal importance during open circuit conditions or during high temperature discharges. During these times the high diffusion coefficient of Ag^+ allows easy migration across the cell into the anolyte. We have explored several ways of maintaining this high concentration gradient across the cell while minimizing the Ag^+ flux into the anolyte.

The first technique studied involved simply increasing l, the thickness of the cell. Fig. 5 illustrates the effect of increasing cell thickness on cell lifetime. While this is one way of increasing cell lifetime, overall cell thickness is limited by the practicalities of battery construction. As is obvious from Equation 4, the thermal environment should play as great a role in determining cell lifetime as overall cell thickness. This effect, shown in Fig. 6, is compounded by the changes in the diffusion coefficient and the electrolyte viscosity as the temperature is changed.

Introducing a layer of chloride anions tends to aid in maintaining the concentration gradient by precipitating any Ag^+ as insoluble AgCl before the Ag^+ ions reach the anode. This 'solution' tends also to emphasize the difficulties involved in using a soluble cathode system since the use of high Cl^- concentrations allow Cl^- diffusion into the catholyte with resulting precipitation of AgCl and loss in cathode performance. Furthermore, the AgCl formed by the Cl^- layer tends to be resistive in nature thus increasing cell *IR* drop.

Another approach to increasing cell performance characteristics is to activate into a load

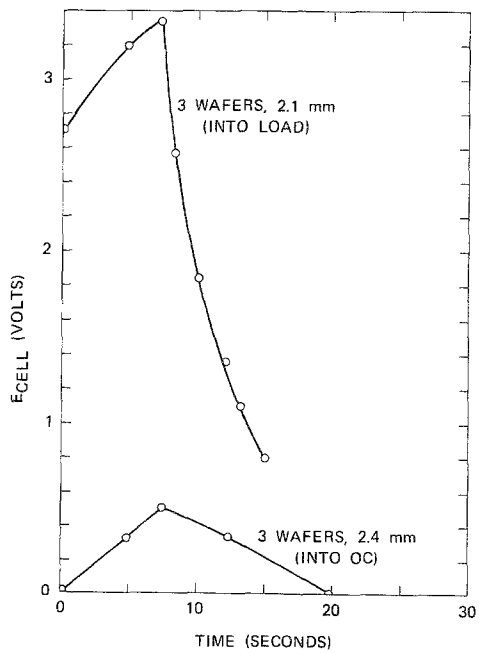

Fig. 7. Effect of activation into load (500 mA cm^{-2}) versus into open circuit. Discharge time dates from application of current (open circuit activation case) or first positive cell voltage (activation into load case). $T \cong 375°C$.

(as opposed to activation into open circuit). By activating into a load, the Ag^+ depletion in the region near the cathode forces Ag^+ migration toward the cathode rather than into the electrolyte. The dramatic illustration of the effect of activation into load is also shown in Fig. 7.

4. Summary

The use of soluble materials in molten nitrate electrolytes is attractive for several reasons including high rate capability and favourable reduction potentials. However, soluble cathodes introduce a new degree of complexity to practical battery cell design.

Factors affecting cell performance include parasitic reactions with binder and cathode material, temperature, concentration and concentration gradients of cathode material, activation into load versus open circuit and the pressure or absence of a chloride layer. Relations have been found with which to evaluate the effect of various factors on the minimal concentration of catholyte required and the effect of various factors on the diffusion of Ag^+ across the cell.

Practical Li(Fe)–$AgNO_3$ cells must operate below about 375° C, use a Cl^- separator wafer, activate into a load and use a catholyte of essentially pure cathode active material in order to sustain current densities at $500\,mA\,cm^{-2}$ for prolonged (90-s) periods.

Acknowledgement

The authors acknowledge financial support from the Naval Sea Systems Command of the US Navy under the task 'High Energy Batteries for Weapons'.

References

[1] G. E. McManis, M. H. Miles and A. N. Fletcher, *J. Electrochem. Soc.* **131** (1984) 283.
[2] M. H. Miles, G. E. McManis and A. N. Fletcher, *Electrochem. Soc. Ext. Abst.* **81-2** (1981) 1405.
[3] *Idem, ibid.* **83-1** (1983) 1176.
[4] M. H. Miles, G. E. McManis and A. N. Fletcher, *J. Electrochem. Soc.* **131** (1984) 2075.
[5] D. E. Harney, US Patent 4 221 849. Assignee: Catalyst Research Corp., Baltimore, MD, 9 September 1980.
[6] G. E. McManis, M. H. Miles and A. N. Fletcher, 'Proceedings Lithium Batteries Symposium, The Electrochemical Society, Pennington, NJ, in press.
[7] Hanspeter Alder, US Patent 3 756 789. Assignee: E. I. Dupont de Nemours and Co., Wilmington, DE, 4 September 1973.
[8] G. E. McManis, M. H. Miles and A. N. Fletcher, *J. Electrochem. Soc.* **131** (1984) 286.
[9] G. E. McManis, M. H. Miles and A. N. Fletcher, 'Proceedings 30th Power Sources Symposium', The Electrochemical Society, Pennington, NJ (1982) pp. 39–41.
[10] A. J. Bard and L. R. Faulkner, 'Electrochemical Methods', John Wiley and Sons (1980) p. 31.
[11] *Idem ibid*, p. 253.
[12] G. J. Janz, C. B. Allen, N. P. Bansal, R. M. Murphy and R. P. T. Tomkins, Physical Properties Date, Compilations Relevant to Energy Storage: II Molten Salts: Data on Single and Multicomposer Salt Systems. NBS-NSRDS Circular 61, Part II, April 1979.